Structure, surface morphology, thermal and flammability characterizations of polyamide6/organic-modified Fe-montmorillonite nanocomposite fibers functionalized by sputter coating of silicon

Yibing Cai [a,b], Ning Wu [a], Qufu Wei [a,*], Kai Zhang [a], Qiuxiang Xu [a], Weidong Gao [a], Lei Song [b], Yuan Hu [b]

[a] Key Laboratory of Eco-textiles, Ministry of Education, Jiangnan University, Wuxi, 214122, Jiangsu, People's Republic of China
[b] State Key Laboratory of Fire Science, University of Science and Technology of China, Hefei, 230027, Anhui, People's Republic of China

ABSTRACT

In the present work, Fe-montmorillonite was synthesized by hydrothermal method, and then was modified by cetyltrimethyl ammonium bromide (CTAB). The polyamide6 (PA6) nanofibers and PA6/organic-modified Fe-montmorillonite (Fe-OMT) nanocomposite fibers were firstly prepared by a facile compounding process with electrospinning, and then coated by silicon nanoparticles (Si) using magnetron sputter technique. The High-resolution transmission electron microscopy (HRTEM) image indicated that the silicate clay layers were well dispersed within the nanocomposite fibers and aligned almost along the axis of the nanofibers. The influences of the Si sputter coating on structures, surface morphology, thermal and flammability properties of PA6 nanocomposite fibers were characterized by Scanning electron microscope (SEM), Energy dispersive X-ray spectroscopy (EDX), X-ray photoelectron spectroscopy (XPS), Atomic force microscope (AFM), Thermogravimetric analyses (TGA) and Micro Combustion Calorimeter (MCC), respectively. The SEM images showed that the diameters of nanocomposite fibers were decreased with the loadings of the Fe-OMT, and the Si thin film with nanoparticles were well coated on the surface of homogeneous and cylindrical nanofibers. The EDX analyses confirmed the presences of the Fe-OMT and Si nanoparticles on the nanofibers. The XPS spectra reflected the chemical features of the deposited nanostructures. The AFM observations revealed a remarkable difference in the surface morphology of nanocomposite fibers after sputter coating. The TGA analyses indicated the barrier effects of silicate clay layers, catalysis effect of Fe^{3+} and synergistic effects between the Fe-OMT and Si improved thermal stability properties of the coated nanocomposite fibers. It was found from the MCC tests that the peak of heat release rate (PHRR) of the coated nanocomposite fibers decreased significantly, contributing to the improved flame retardant properties.

© 2008 Elsevier B.V. All rights reserved.

1. Introduction

Polymer nanofibers have interesting properties which are the result of their extremely high ratio of surface to weight compared to the other conventional fibrous structures. These make nanofibers ideal for use in such applications as filtration, sensor, protective clothing and functional materials, attributed to the high pore volume and tight pore sizes [1–7]. Polyamide 6 (PA6) is one of the most important engineering polymers manufactured in large quantities in various forms, such fibers, films, and plastics for various applications. PA6 accounts for a majority of the commercial polyamide production and application. The improvement of thermal and flammability properties of polymer nanofibers is a major concern in many practical applications. The polymer/clay nanocomposite technology is believed to be a new promising approach in fire retardancy due to their great potential in forced flaming conditions, for instance the reduction of

the flame spread and fire propagation. The most frequently used clay is montmorillonite, MMT, which is an aluminous silicate mineral with sodium ions between the clay layers. The PA6 nanocomposites, loaded with only 1.6 wt.% clay silicate layers, exhibited high strength, high modulus, high heat distortion temperature and low gas permeability compared to pure PA6 [8]. It was reported that the mechanical properties of the electrospun PA6/Na-montmorillonite fibrous mats were significantly improved, compared to the pure PA6 fibrous mats which was well studied using an atomic force microscope (AFM) [4].

Then, the phenomenon of isomorphous replacement in montmorillonite is very common. The Si^{4+} in the tetrahedral crystal lattice of structural level is replaced by Al^{3+}. The Al^{3+} in the octahedral lattice is replaced by Fe^{3+}, Fe^{2+}, Mg^{2+}, Cr^{3+}, Zn^{2+} and Li^+ etc. Due to exchange of unequal values, the electric neutrality of the structure is destroyed and some excess electrons may appear. These electrons are compensated by alkali metal cations or alkali earth metal cations, and the cations of compensation come into spaces between structure levels and distribute into the edges of lattices. Those cations are often replaced by other cations, so the clay performs some sort of distinctive functions. These

types of MMT may possess different performances from natural MMT [9]. For example, the catalysis effect of Cu^{2+}-exchanged and Fe^{3+}-exchanged montmorillonite (Cu^{2+}-MMT, Fe^{3+}-MMT) increased remarkably the charred residue of nylon6 nanocomposites [10].

The sputtering technology has been widely used to deposit very thin films on various substrates for commercial and scientific purposes [11]. The ability to deposit well-controlled coatings on nanofibers would expand the application of nanofibers, based on changes to both the physical and chemical properties of the nanofibers. The emerging nanoparticles which have shown promising effects on polymer thermal degradation are metal oxides particles (i.e. Al_2O_3, TiO_2 and Fe_2O_3) [12,13] and inorganic nanoparticles (i.e., Si). The use of particles in the submicronic or nanometric range as synergistic agents in addition to usual fire retardant additives seems to be very promising. The silicon may be considered as a universal additive to improve the fire-retardant properties of polymers and decrease the harmful impact on environmental safety [14,15]. It has also been noticed that their nanometric size made them suitable for synergistic effects with organoclays, allowing thermal and fire behavior performances to be improved. In the present work, the Fe-montmorillonite was firstly hydrothermal synthesized [9,16,17] and then was modified by cetyltrimethyl ammonium bromide (CTAB). The difference between Fe-MMT and natural MMT was that Fe (III) ion replaced Al (III) ion in the crystal lattice of the MMT. The PA6/organic-modified Fe-montmorillonite (Fe-OMT) composite solution was electrospun to form nanocomposite fibers and then was deposited with Si nanoparticles by magnetron sputter coating. The effects of Si sputter coating on structure and surface morphology were observed by SEM, EDX, XPS and AFM. The thermal stability and flame retardant properties of the nanocomposite fibers before and after sputtering coating Si were also characterized by TGA and MCC.

2. Experimental

2.1. Materials

Polyamide6 (PA6, 1003NW8, with weight-average molecular weight 18000, characteristic viscosity was 2.8) was supplied as pellets by UBE Industries, Japan. The acidic sodium silicate ($Na_2SiO_3 \cdot 9H_2O$), iron (III) chloride ($FeCl_3 \cdot 6H_2O$), zinc acetate [$Zn(CH_3COO)_2 \cdot 2H_2O$] and sodium hydroxide (NaOH) were obtained from the Shanghai Chemical Regents Company. The 99.5% N, N-dimethyl formamide (DMF), 88% formic acid and cetyltrimethyl ammonium bromide (CTAB) were all used as received. All chemicals were of analytical grade and were used as received without further purification.

2.2. Synthesis of organic-modified Fe-montmorillonite (Fe-OMT)

The Fe-MMT was synthesized as follows: hydrous oxide was prepared by mixing $Na_2SiO_3 \cdot 9H_2O$ with $FeCl_3 \cdot 6H_2O$ and $Zn(CH_3COO)_2 \cdot 2H_2O$ solutions to set the atomic ratio at Si/Fe/Zn = 4:1.7:0.3 (refer to previous reports for a detailed method of synthesis [9,17]). And the CEC of the Fe-MMT was 102 meq/100 g.

Then, the synthesized Fe-MMT was dispersed in water and formed a suspension by vigorous stirring. The appropriate amount of CTAB was added to the suspension and stirred for 3 h at 80 °C. The suspension was centrifuged and washed with boiling distilled water to remove the excess CTAB, until the supernatant liquid was tested by a 0.1 mol/l $AgNO_3$ solution without yielding sedimentation. The product was then dried in vacuum and ground into powder to get the organic-modified Fe-montmorillonite (Fe-OMT).

2.3. Preparation of electrospun nanocomposite fibers

The slurry was prepared by dispersing Fe-OMT (0.6960 g) powder into DMF (20.00 ml) solvent using magnetic stirring for 30 min until the powder uniformly dispersed in the DMF, and then was sonicated for 1.5 h. 15 wt.% of PA6 dissolved in formic acid was also prepared. The prepared clay slurry was then put into the PA6 solution, which was mixed by magnetic stirring for 30 min and then was sonicated for another 20 min. The polymer solutions were electrospun at a positive voltage of 14 kV with a working distance of 10 cm (the distance between the needle tip and the collection plate), and an ejection rate of 0.5 ml/h. The mass ratio of the Fe-OMT to PA6 was 4 wt.%, and the electrospun fibers was referred to as PA6/Fe-OMT nanocomposite fibers.

2.4. Sputter coating

A magnetron sputter coating system JZCK-420B (Shenyang, Juzhi Co., Ltd.) was used to deposit a thin film on the nanocomposite fibers. A high purity silicon target (99.999%) was mounted on the cathode, and the nanofibers substrate was placed on the anode facing the target. Argon pressure was set at 0.5 Pa. The radio frequency (RF) power used for silicon sputtering was set at 120 W. The thickness of the deposition layer was 100 nm, which was measured using a FTM-V in-situ film thickness monitor.

2.5. Characterization

To investigate the dispersion of the clay layers within the nanocomposite fibers, the PA6/Fe-OMT nanocomposite fibers were directly electrospun onto a 200-mesh Cu grid and observed by a High-resolution transmission electron microscopy (HRTEM, JEOL 2010) with an accelerating voltage of 200 kV.

Scanning electron microscope (SEM) Quanta 200 was used to examine the structure of the nanocomposite fibers. The samples were coated with a thin layer of gold by sputtering before the SEM imaging. The SEM Quanta 200 equipped with Energy dispersive X-ray spectroscopy (EDX) was used to examine the chemical compositions of the sputter coated nanofibers. An accelerating voltage of 20 kV with accounting time of 100 s was applied.

X-ray photoelectron spectra (XPS) analysis was performaced on a photoelectron spectrometer (ESCA Lab MK II instrument, UK) using Mg-Kα radiation as the exciting source. Atomic force microscope (AFM) was used to further observe the surface morphology of the nanocomposite fibers. The AFM used in this work was a Benyuan CSPM 4000. Scanning was carried out in tapping mode. All images were obtained at ambient conditions.

Thermogravimetric analyses (TGA) were carried out using a TGA50H thermo-analyzer instrument from 25 to 700 °C using a linear heating rate of 10 °C/min under nitrogen flow. The nitrogen flow was 25 ml/min. Samples were measured in a sealed alumina pan with a mass of about 10 mg.

Flammability property was characterized by Micro Combustion Calorimeter (MCC) based on the principle of oxygen consumption. The signals from the MCC were recorded and analyzed by a computer system. The samples were firstly heated with a linear heating rate of 1 °C/s in pyrolyzed furnace. The decomposed products were brought away by inert gases, then were mixed with oxygen and came to the combustion chamber at 900 °C. Finally, the mixed gases were completely oxidated. The mass of samples for the MCC tests was about 4–6 mg.

3. Results and discussion

3.1. Structure and morphology

The HRTEM was used to investigate the dispersion of silicate clay platelets within the PA6 nanocomposite fibers. The HRTEM image revealed that the silicate clay platelets were well dispersed within the electrospun PA6 nanocomposite fibers, and the silicate clay layers
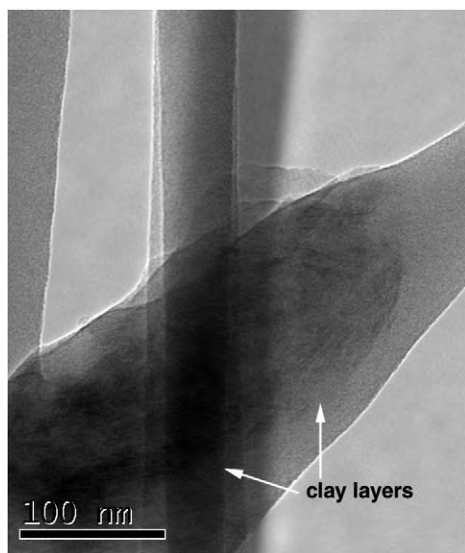
Fig. 1. HRTEM image of the PA6/Fe-OMT nanocomposite fibers.

were almost oriented in the fiber axial direction, as indicated in Fig. 1. This was attributed to the higher draw ration that imparted a larger stress on the fiber as it was being formed during the electrospinning process, contributing to a proper alignment of the two-dimensional nanoclays along the fiber axis. Meanwhile, the orientation also confirmed that extensional forces were exerted on the nanocomposite fibers during electrospinning.
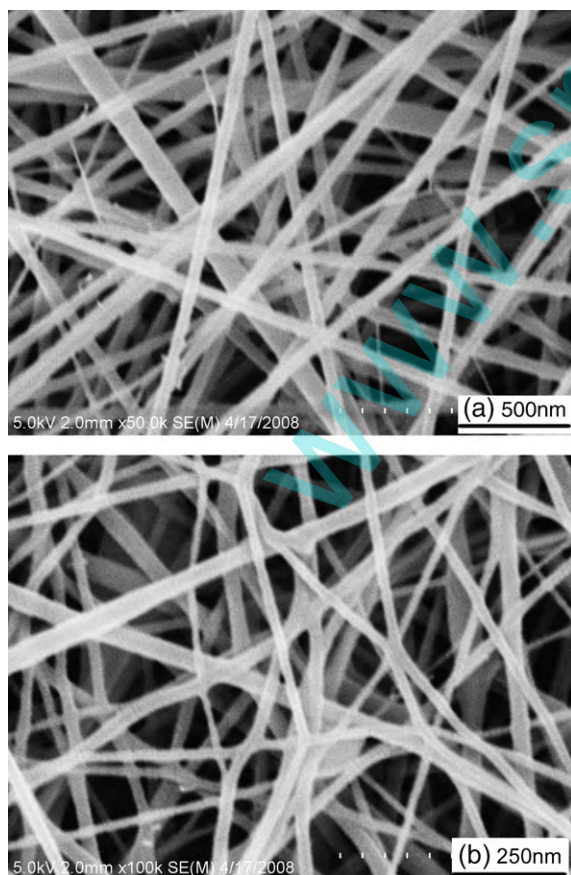
The SEM images of electrospun PA6 nanofibers and PA6/Fe-OMT nanocomposite fibers before sputter coating, collected on the aluminum foil, are illustrated in Fig. 2. The nanofibers were randomly distributed to form the three-dimensional fibrous web. It was observed that the electrospun nanofibers possessed variable fiber diameters. The morphology and average diameter of the electrospun PA6/Fe-OMT nanocomposite fibers were significantly affected by the loadings of Fe-OMT. The average diameters of the PA6/O-MMT nanocomposite fibers (Fig. 2b) were decreased compared to those of the PA6 nanofibers (Fig. 2a). The SEM images of sputter coated nanofibers are also shown in Fig. 3. It was observed that the Si nanoparticles were well deposited on the surface of nanofibers and formed a thin film. The SEM images also revealed that the sputtered Si nanoparticles on the PA6/Fe-OMT nanocomposite fibers looked smoother, compacter and more uniform than those on the PA6 nanofibers. It was believed that the loading of the Fe-OMT reduced the interface tensions between the nanofibers and the Si nanoparticles, and was propitious to the deposition of Si nanoparticles. It was found from SEM images that the fiber diameters of the coated PA6/Fe-OMT nanocomposite fibers were decreased to about 100–200 nm (Fig. 3b) compared to the coated PA6 nanofibers with an average diameter of about 200–300 nm, as indicated in Fig. 3a. This was because the loading of quaternary ammonium salts as an organic modifier increased the charge density in ejected jets and thus stronger elongation forces were imposed to the jets because of the self-repulsion of the excess charges under the electrical field, resulting in substantially straighter shape and smaller diameter of electrospun fibers. Meanwhile, the conductivity of the PA6 solution was another major factor affecting the morphology and diameter of the electrospun PA6 nanofibers. The quaternary ammonium ion ($C_{16}H_{33}(CH_3)_3N+$) within the silicate clay layers and cations (i.e., Na^+ and Zn^{2+}) located

Fig. 2. SEM images of (a) PA6 nanofibers and (b) PA6/Fe-OMT nanocomposite fibers.
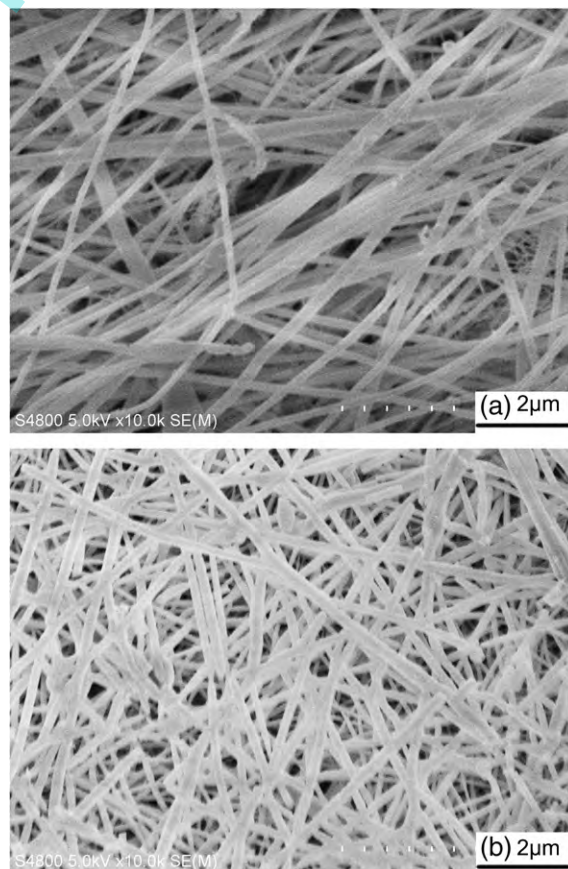
Fig. 3. SEM images of (a) coated PA6 nanofibers and (b) coated PA6/Fe-OMT nanocomposite fibers.

between MMT layers, improved the conductivity of PA6/Fe-OMT composite solutions [18–20], leading to the decrease in the average diameter of the PA6/Fe-OMT nanocomposite fibers.

3.2. EDX characterization

Fig. 4 shows the EDX spectra of the (a) PA6/Fe-OMT nanocomposite fibers, (b) coated PA6 nanofibers and (c) coated PA6/Fe-OMT nanocomposite fibers. Fig. 4a indicates that the PA6/Fe-OMT nanocomposite fibers mainly consisted of C, O, Fe, Zn and Si, and further confirmed the presence of the Fe-OMT within the nanocomposite fibers. The sputter coated nanoparticles on the surface of the PA6 nanofibers were also confirmed by EDX analyses. It can be seen from Fig. 4b that the coated PA6 nanofibers dominantly consisted of C, O and Si, derived from the PA6 and the sputter coated Si nanoparticles, respectively. Fig. 4c reveals the presences of Fe, Zn and Si for the coated PA6/Fe-OMT nanocomposite fibers, derived from the contribution of the Fe-OMT within the nanocomposite fibers. Compared to the PA6 nanocomposite fibers (Fig. 4a), the Si amount in the coated PA6 nanofibers and coated PA6/Fe-OMT nanocomposite fibers had remarkable increases, as illustrated in Fig. 4b and c. This was attributed to the sputter coated Si nanoparticles on the surface of the nanocomposite fibers.

3.3. XPS analysis

XPS analysis revealed the compositions of the nanofibers surfaces. The XPS spectra of (a) PA6/Fe-OMT nanocomposite fibers, (b) coated
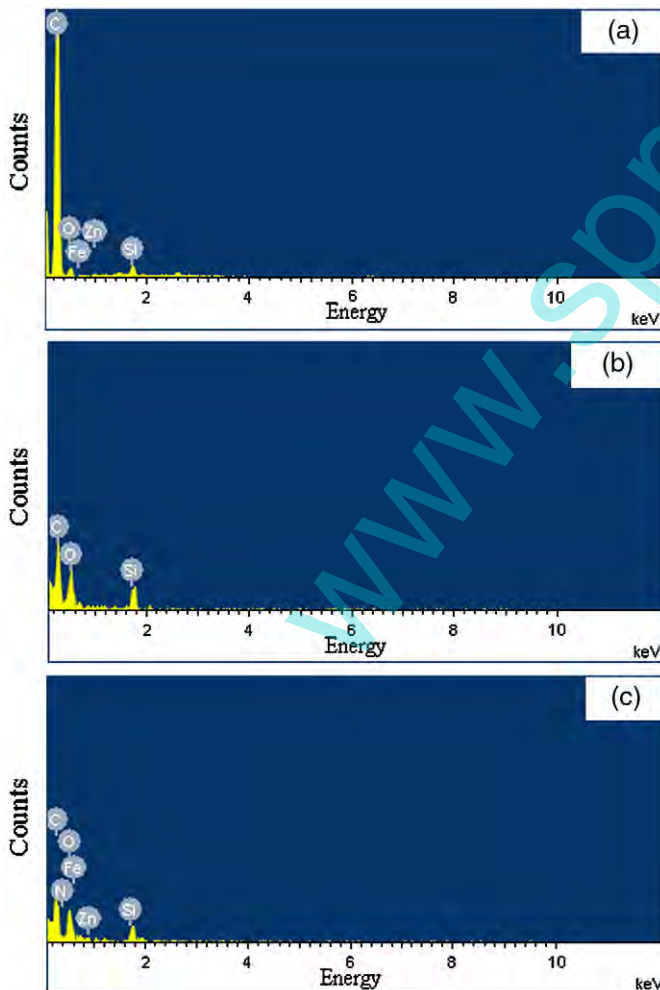
Fig. 4. EDX spectra of (a) PA6/Fe-OMT nanocomposite fibers, (b) coated PA6 nanofibers and (c) coated PA6/Fe-OMT nanocomposite fibers.
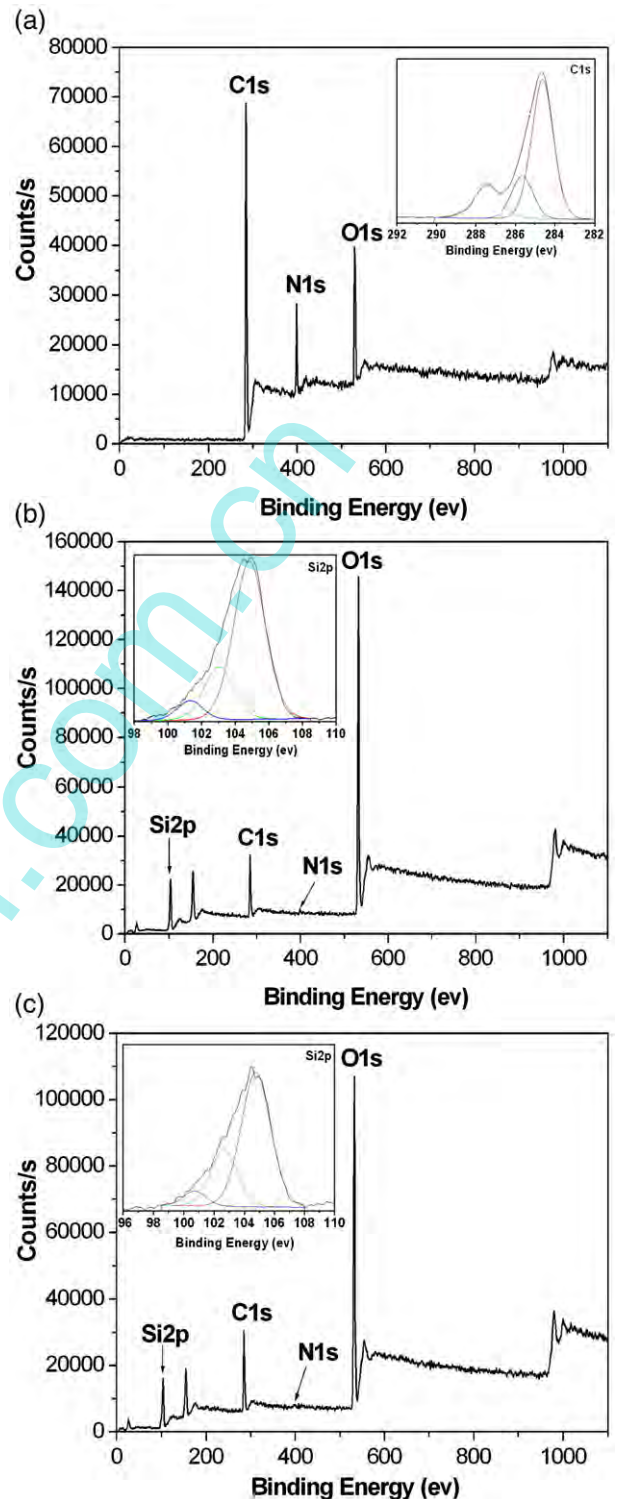
Fig. 5. XPS spectra of (a) PA6/Fe-OMT nanocomposite fibers (the inset illustrates the XPS spectra of the C_1s), (b) coated PA6 nanofibers (the inset illustrates the XPS spectra of the Si_2p) and (c) coated PA6/Fe-OMT nanocomposite fibers (the inset illustrates the XPS spectra of the Si_2p).

PA6 nanofibers and (c) coated PA6/Fe-OMT nanocomposite fibers are shown in Fig. 5. It can be seen from Fig. 5a that the main peaks were C_1s, N_1s and O_1s centered at 284.5, 399.1 and 530.7eV, respectively. Meanwhile, the binding energies at 104.1eV for Si_2p, 52.0eV for Fe_3p and 1022.2eV for Zn_2p of layer silicate clay could almost not be detected [21]. The result confirmed that the silicate clay was not accumulated on the surface of nanocomposite fibers and was well

dispersed within the composite nanofibers. It was also observed from Fig. 5b that the main contents of the surface species of coated PA6 nanofibers were C, N, O and Si. The presence of the Si_2p peak corresponding to the binding energy at about 104.1 eV indicated that Si nanoparticles were formed on the surfaces of the nanofibers, as indicated in Fig. 5b. Comparing to the XPS spectrum of the PA6/Fe-OMT nanocomposite fibers (Fig. 5a), Fig. 5c shows that the binding energies at 104.1 eV for the Si_2p peak assigned to the sputter coated Si nanoparticles. Moreover, the peaks of the Si_2p, Fe_3p and Zn_2p derived from the Fe-OMT could not be found in Fig. 5c. This result also indicated that the silicate clay was well dispersed within the nanocomposite fibers and the Si nanoparticles were deposited on the surface of nanocomposite fibers.

3.4. Surface morphology

The surface morphology of electrospun nanofibers after sputter coating was investigated using AFM. The AFM images of the coated PA6 nanofibers and coated PA6/Fe-OMT nanocomposite fibers are presented in Fig. 6. The three-dimensional fibrous webs consisted of many
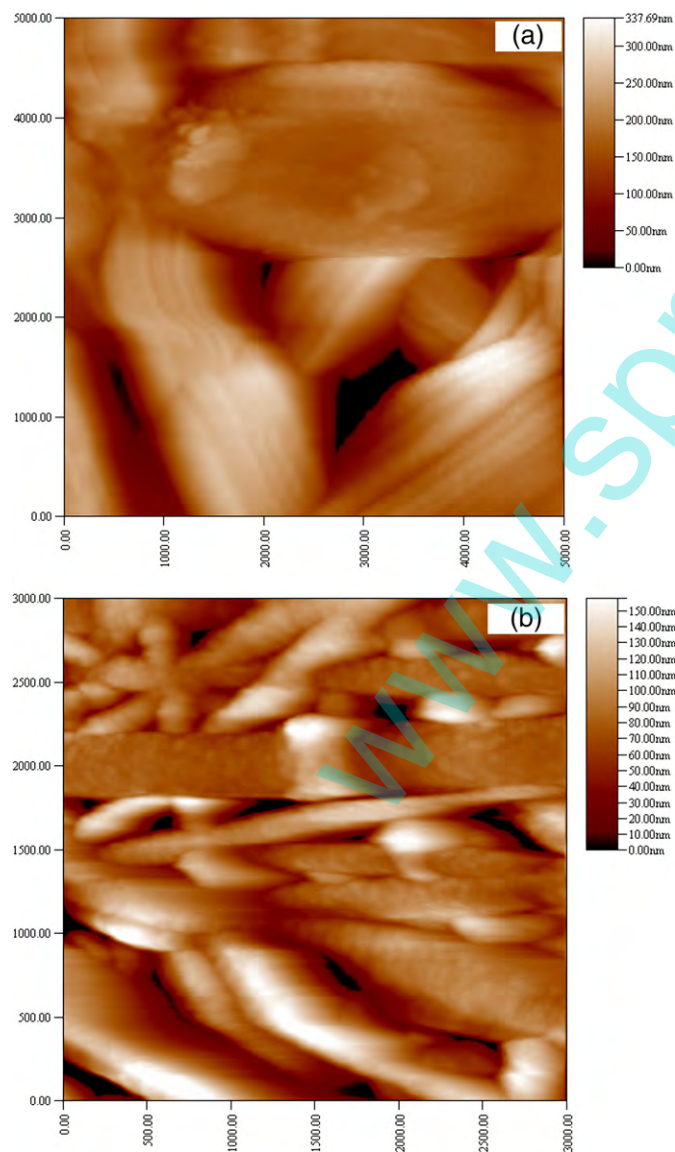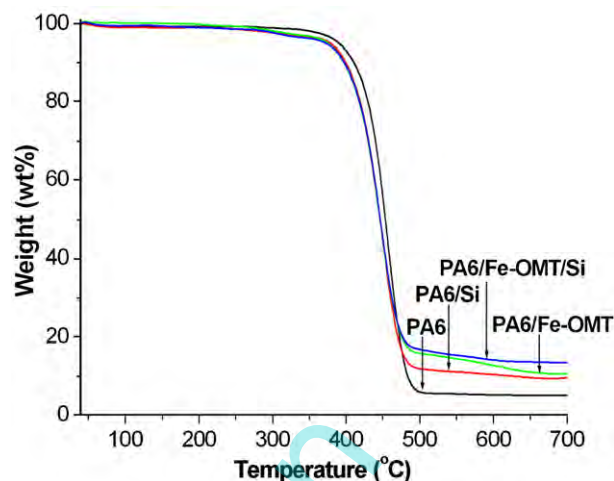
Fig. 7. TGA curves of the PA6 nanofibers, PA6/Fe-OMT nanocomposite fibers, coated PA6 nanofibers and coated PA6/Fe-OMT nanocomposite fibers.

individual nanofibers with variable diameters and the fibers were randomly oriented in the web. The AFM image revealed the relatively smooth surface with clear fibril structures of the fiber surface. It was attributed to the effects of drawing and high shear flow during electrospinning. Sputter coating significantly altered the surface characteristics of the nanofibers. It can be seen that the Si nanoparticles were quite uniformly distributed on the surface of the nanofibers. The Si nanoparticles with variable sizes formed the rougher surface after sputter coating. It can be seen from Fig. 6a that the Si nanoparticles formed a thinner film on the surface of the PA6 nanofibers. The adhesion between the Si nanoparticles and PA6 nanofibers looked loose and the surface was scraggly. Compared to the PA6 nanofibers, however, the Si nanoparticles coated on the surface of the PA6/Fe-OMT nanocomposite nanofibers appeared compacter, as indicated in Fig. 6b. The reasons may be that the loading of the Fe-OMT reduced the interface tensions between the Si nanoparticles and the PA6 nanofibers, facilitating the depositions of Si nanoparticles. The smoothness of the Si thin film was improved and the sputtered film became compacter and homogeneous.

3.5. Thermal stability properties

Thermal stability properties of the electrospun nanofibers before and after sputter coating were evaluated using TGA in nitrogen atmosphere. The TGA curves for PA6 nanofibers, PA6/Fe-OMT nanocomposite fibers, coated PA6 nanofibers and coated PA6/Fe-OMT nanocomposite fibers are shown in Fig. 7. It can be seen that the PA6 nanofibers before and after sputter coating displayed a one step degradation. The oneset degradation temperatures (defined as the temperature at 5 wt.% weight loss) were 390.4 °C (PA6 nanofibers), 375.1 °C (PA6/Fe-OMT nanocomposite fibers), 378.3 °C (coated PA6 nanofibers) and 372.7 °C (coated PA6/Fe-OMT nanocomposite fibers), respectively. Compared to the PA6 nanofibers, the onset thermal stability of the PA6/Fe-OMT nanocomposite fibers showed a slight decrease. Moreover, the thermal stability of coated PA6/Fe-OMT nanocomposite fibers was slightly lower than that of the coated PA6 nanofibers. The reasons may be that the Fe^{3+} cations located on the Fe-OMT catalyzed the onset degradation of PA6 and decreased the thermal stability of PA6 nanofibers. The effect was attributed to the ability of the cation to form complexes in which the metal atoms were coordinately bonded to the carbonyl oxygen atom of the amide group and were surrounded by polar solvent molecules [22]. It was also suggested that Fe^{3+} cations facilitated decomposition of hydroperoxides through a reversible oxidative–reductive catalytic process between Fe^{3+} and Fe^{2+} [23]. Meanwhile, the alkylammonium cations

Fig. 6. AFM images of the (a) coated PA6 nanofibers and (b) coated PA6/Fe-OMT nanocomposite fibers.

were thermal instability and degraded in advance. The alkylammonium cations in the Fe-OMT could suffer decomposition following the Hofmann elimination reaction [24,25], and its product would catalyze the degradation of PA6. Furthermore, the clay itself could also catalyze the degradation of polymer materials [26]. These aspects would decrease the thermal stability of PA6 nanocomposite fibers before and after sputter coating.

However, the yield of the charred residue at 700 °C for the coated PA6/Fe-OMT nanocomposite fibers was increased to 13.42% from 10.56% for PA6/Fe-OMT nanocomposite fibers and 9.48% for the coated PA6 nanofibers. The reasons may be that the cations of some transition metals (e.g., Fe^{3+}) promoted the molecular crosslinking and increased the charred residue. Besides, the Fe ion was also the operative site for radical trapping during the thermal degradation of the nanocomposite fibers [27]. It was also known that transition metal halides including ferric chloride could thermally lose a halogen atom; for example, $FeCl_3$ was easily reduced to lower-valent species such as $FeCl_2$ upon heating. This reaction should be accelerated by the additional silicon, which could act as a reducing agent [23,28]. The resulting silicon tetrachloride (i.e., oxidized from of silicon) could readily hydrolyze (crystal water released form the collapse of the Fe-OMT) to generate hydrogen chloride and silicon dioxide [29]. The detailed reactions were as follows:

$$2MetCl_2 + nSi \rightarrow 2Met(0) + (n-1)Si + SiCl_4$$

$$SiCl_4 + 2H_2O \rightarrow 4HCl + SiO_2$$

The in-situ generated silicon dioxide may also contribute to enhancing the char formation. The increased charred residue contributed to the improved thermal stability of the coated PA6/Fe-OMT nanocomposite fibers. Meanwhile, this was also attributed to the silicate clay layers which could presumably facilitate the reassembly of lamellas to form three-dimensional char, which might occur on the surface of the nanofibers and create a physical protective barrier. Moreover, the silicate clay layers could act as a superior insulator and mass-transport barrier and subsequently mitigate the escape of volatile products generated during the thermal decomposition, contributing to the improved thermal stability properties of PA6 nanocomposite fibers [3,30].

3.6. Flammability properties

The Micro Combustion Calorimeter (MCC) was one of the most effective bench scale methods for investigating the combustion properties of polymer materials. The peak of heat release rate (PHRR) has been found to be one of the most important parameters to evaluate fire safety [31,32]. The flammability properties of the PA6 nanocomposite fibers before and after sputter coating Si were characterized by MCC in the present work. The HRR curves of the PA6 nanofibers, coated PA6 nanofibers, PA6/Fe-OMT nanocomposite fibers and coated PA6/Fe-OMT nanocomposite fibers are illustrated in Fig. 8. The PHRR of the PA6/Fe-OMT nanocomposite fibers decreased to 554.4 W/g from 680.7 W/g for the PA6 nanofibers, attributed to the barrier effect of the silicate clay. After sputter coating Si, the PHRR decreased to 601.3 W/g (coated PA6 nanofibers) and 511.1 W/g (coated PA6/Fe-OMT nanocomposite fibers), respectively, compared to the PA6 nanofibers. The reasons may be that the in-situ generated silicon dioxide and the reassembly of lamellas for silicate clay layers coated on the surface of the nanofibers created a physical protective barrier, which could act as a superior insulator and mass-transport barrier. Meanwhile, the remarkable decreases of the PHRR for coated PA6/Fe-OMT nanocomposite fibers were also due to the synergistic effects between the Fe-OMT and Si. Moreover, it should be noted that the time to ignite the PA6 nanocomposite fibers were both relatively short in comparison with PA6 nanofibers before and after sputter coating Si. The initial HRR for the PA6 nanocomposite fibers were both higher than PA6 nanofibers before arriving at the peaks of heat release rate,
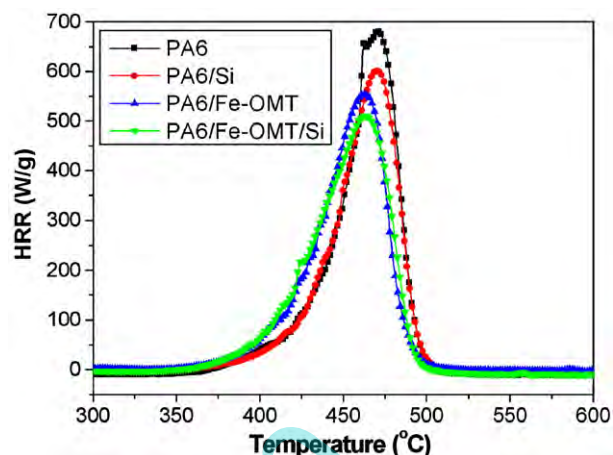
Fig. 8. HRR curves of the PA6 nanofibers, PA6/Fe-OMT nanocomposite fibers, coated PA6 nanofibers and coated PA6/Fe-OMT nanocomposite fibers.

probably because of thermal decomposition of cationic surfactants (CTAB), resulting in the formation of volatile combustibles [32].

4. Conclusions

The PA6/Fe-OMT nanocomposite fibers were prepared by a facile compounding and electrospinning. The surface functionalization of nanocomposite fibers was made by depositing well-controlled Si nanoparticles using sputter coating. The structures of nanocomposite fibers characterized by HRTEM indicated that the silicate clay layers were partially exfoliated and aligned along the axis of the nanofibers. The influences of Si nanoparticles on structural characteristics, surface morphology thermal stability and flammability properties of the nanocomposite fibers were investigated. The SEM images showed that the diameters of nanocomposite fibers decreased with the loadings of the Fe-OMT and the Si nanoparticles well coated on the surface of homogeneous and cylindrical nanofibers. The XPS and EDX confirmed the presence of the Fe-OMT within the nanocomposite fibers and indicated the physical-chemical features of the deposited nanostructures. The AFM observations indicated that there was a remarkable difference in the surface morphology of nanofibers after sputter coating. The loadings of the Fe-OMT led to the compact and homogeneous deposition of the Si nanoparticles, due to the decreased interface tensions. The TGA results revealed the improved thermal stability properties of the coated nanocomposite fibers, attributed to the superior insulator, mass-transport and physical protective barriers of silicate clay layers, catalysis effect of Fe^{3+} and synergistic effects between the Fe-OMT and Si nanoparticles. It was found from the MCC tests that the PHRR of the coated PA6 nanocomposite fibers decreased notably due to the in-situ generated silicon dioxide, barrier effects of silicate clay and the synergistic effects between the Fe-OMT and Si, contributing to the improved flame retardant properties.

References

[1] H. Fong, W.D. Liu, C.S. Wang, R.A. Vaia, Polymer 43 (2002) 775.
[2] J.H. Hong, E.H. Jeong, H.S. Lee, D.H. Baik, S.W. Seo, J.H. Youk, J. Polym. Sci., B, Polym. Phys. 43 (2005) 3171.
[3] M. Wang, A.J. Hsieh, G.C. Rutledge, Polymer 46 (2005) 3407.

[4] L. Li, L.M. Bellan, H.G. Craighead, M.W. Frey, Polymer 47 (2006) 6208.
[5] G.M. Kim, G.H. Michler, F. Ania, F.J. Balta Calleja, Polymer 48 (2007) 4814.
[6] Y. Ji, B.Q. Li, S.R. Ge, J.C. Sokolov, M.H. Rafailovich, Langmuir 22 (2006) 1321.
[7] K.H. Yoon, M.B. Polk, B.G. Min, D.A. Schiraldi, Polym. Int. 53 (2004) 2072.
[8] N. Hasegawa, H. Okamoto, M. Kato, A. Norio Sata, Polymer 44 (2003) 2933.
[9] Q.H. Kong, Y. Hu, L. Yang, Z.Y. Chen, W.C. Fan, Polym. Compos. 27 (2006) 49.
[10] J. Liu, Y. Hu, S.F. Wang, L. Song, Z.Y. Chen, W.C. Fan, Colloid Polym. Sci. 282 (2004) 291.
[11] Q.F. Wei, Q.X. Xu, Y.B. Cai, Y.Y. Wang, Surf. Coat. Technol. 202 (2008) 4673.
[12] A. Laachachi, E. Leroy, M. Cochez, M. Ferriol, J.M. Lopez-Cuesta, Polym. Degrad. Stab. 89 (2005) 344.
[13] A. Laachachi, M. Cochez, E. Leroy, P. Gaudon, M. Ferriol, J.M. Lopez-Cuesta, Polym. Adv. Technol. 17 (2006) 327.
[14] G.E. Zaikov, S.M. Lomakin, Polym. Degrad. Stab. 54 (1996) 223.
[15] R.J.H. Voorhoeve, Organohalosilanes precursors to silicones, Elsevier, Amsterdam, 1967.
[16] T. Nagase, T. Iwasaka, T. Ebina, H. Hayashi, Y. Onodera, N.C. Dutta, Chem. Lett. 4 (1999) 303.
[17] Q.H. Kong, Y. Hu, L. Song, Y.L. Wang, Z.Y. Chen, W.C. Fan, Polym. Adv. Technol. 17 (2006) 463.
[18] X.H. Zong, K. Kim, D.F. Fang, S.F. Ran, B.S. Hsiao, B. Chu, Polymer 43 (2002) 4403.
[19] W.K. Son, J.H. Youk, T.S. Lee, W.H. Park, Polymer 45 (2004) 2959.
[20] J.S. Choi, S.W. Lee, L. Jeong, S.H. Bae, B.C. Min, J.H. Youk, W.H. Park, Int. J. Biol. Macromol. 34 (2004) 249.
[21] Y.B. Cai, F.L. Huang, Q.F. Wei, E.C. Wu, W.D. Gao, Appl. Surf. Sci. 254 (2008) 5501.
[22] P. Dunn, G.F. Sansom, J. Appl. Polym. Sci. 13 (1969) 1657.
[23] N.S. Allen, M.J. Harrison, M. Ledward, G.W. Fellows, Polym. Degrad. Stab. 23 (1989) 165.
[24] J. Zhu, A.B. Morgan, F.J. Lamelas, C.A. Wilkie, Chem. Mater. 13 (2001) 3774.
[25] W. Xie, Z.M. Gao, W.P. Pan, R. Vaia, D.L. Hunter, A. Singh, Polym. Mater. Sci. Eng. 83 (2000) 284.
[26] C.G. Zhao, H.L. Qin, F.L. Gong, M. Feng, S.M. Zhang, M.S. Yang, Polym. Degrad. Stab. 87 (2005) 183.
[27] J. Zhu, C.A. Wilkie, Chem. Mater. 13 (2001) 4649.
[28] J.W. Jang, J.W. Kim, J.Y. Bae, Polym. Degrad. Stab. 90 (2005) 508.
[29] N.I. Sax, R.J. Lewis, Dangerous properties of industrial materials, 7th ed. Van Nostrand Reinhold, New York, 1989.
[30] J.W. Gilman, C.L. Jackson, A.B. Morgan, R. Harris, E. Manias, E.P. Giannelis, Chem. Mater. 12 (2000) 1866.
[31] J.W. Gilman, Appl. Clay Sci. 15 (1999) 31.
[32] M. Zanetti, T. Kashiwagi, L. Falqui, G. Camino, Chem. Mater. 14 (2002) 881.